Memoirs of the Faculty of Science, Kyoto University, Series of Physics, Astrophysics, Geophysics and Chemistry, Vol. XXXVI, No. 1, Article 6, 1981

PRODUCTION OF ELECTRON PAIRS IN PROTON-NUCLEUS COLLISIONS AT 13 GeV/c

By

Shu NAITO

Department of Physics, Kyoto University, Kyoto

(*Received March 20, 1980*)

ABSTRACT

We have measured the mass distribution of the dilepton production in proton-nucleus collision.

The electron pair productions in the collision of protons with a Be target were measured at the incident momentum of 13 GeV/c. The measurement was performed in the region of electron pair mass between 0.3 and 1.3 GeV, and of nearly $y=0$ in the centre of mass system of the incident proton and a single nucleon in the target nucleus.

We have observed a large yield of electron pairs in the low mass region, exceeding a simple extrapolation of the Drell-Yan prediction. The results are also compared with some theoretical models proposed to explain the dilepton production in the low mass region, and the related discussions are given.

I. Introduction

The subject of this paper is the study of lepton pair production at low pair mass in proton-nucleus collisions.

The experiments were performed at the National Laboratory for High Energy Physics (KEK), the reactions studied are

$$p+Be \longrightarrow e^+e^-+X \qquad \text{(I–1)},$$

$$p+Be \longrightarrow e^{\pm}+X \qquad \text{(I–2)}.$$

The momentum of incident proton was 13 GeV/c for the reaction (I–1), and 8, 9 and 13 GeV/c for the reaction (I–2). These experiments were performed at the slow-extracted beam line of the KEK proton synchrotron with a double arm spectrometer. In this report we describe the result of the experiment for the reaction (I–1). The results of the experiment for the reaction (I–2) will be reported elsewhere.

The study of lepton pair production in the hadron-hadron collision gives the useful information to probe the internal structure, especially the electromagnetic structure of hadrons[1].

We probe the electromgagnetic structure of nucleons by studying the dilepton continuum via a virtual photon production, as is shown in Fig. I–1–a. This process is analogous to the deep inelastic lepton-nucleon scattering (Fig. I–1–b), where the virtual photon is spacelike[2]. However, the virtual photon of our case is timelike. In the both cases, a known probe which is the photon is used to study the nucleon electromagnetic structure. The lepton-photon vertex is totally understood by the quantum electrodynamics (QED). It is then the photon-hadron vertex is the subject to be explored here. Measurements of the hadronic vertex function give us the

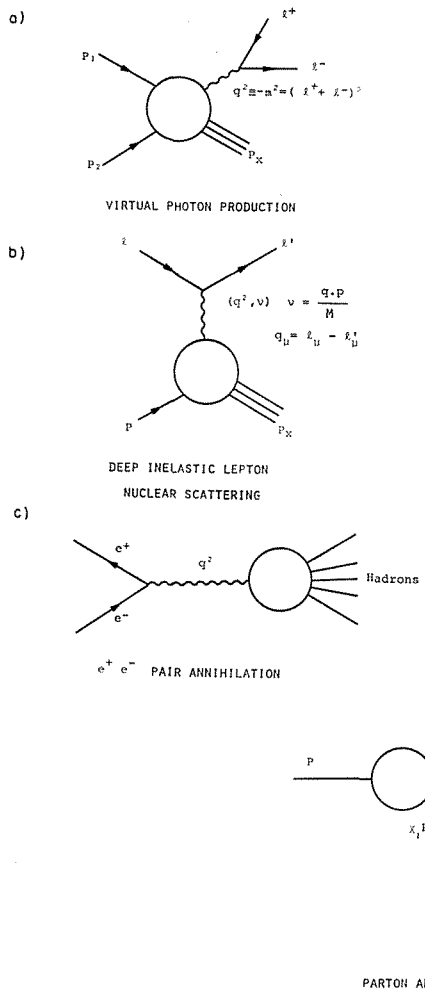

Fig. I–1 a) Inclusive virtual phton production in hadronic collisions.
b) Deep inelastic lepton nucleon scattering.
c) Hadron production in e^+e^- annihilation.

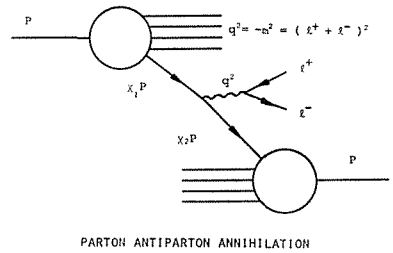

Fig. I–2 Drell-Yan model for massive lepton pair production by partonantiparton annihilation.

information about the nucleon structure. Another related process is the hadron production in colliding e^+e^- beam experiments (see Fig. I–1–c) where the photon is again timelike.

There are many theoretical models to describe how a photon interacts with hadrons. The quark-parton model as developed by Bjorken[4] is the most studied one among these models. The hadron consists of the pointlike constituents called "partons". These partons interact with each other in the collision process. This decomposition allows to calculate exactly the hadronic vertex in terms of QED. This picture of hadrons can easily be shown to predict the Bjorken scaling low in deep inelastic lepton nucleon scattering; that is, the cross section can be expressed with a function of $x=q^2/2Mv$ (see Fig. I–1–b), instead of both q^2 and v.

Drell and Yan showed how massive lepton pairs could be produced in hadron-hadron collisions using the parton model. Their model is shown in Fig. I–2. In this model, the differential cross section can be expressed as the following,

$$\frac{d^2\sigma}{dmdy}=\frac{1}{3}\cdot\frac{8\pi\alpha^2}{3m^3}\cdot\sum_i \lambda_i^2 f_{1i}(x_1)\bar{f}_{2i}(x_2) \qquad \text{(I-3)},$$

where m is the lepton pair mass, y is the rapidity of virtual photon in the nucleon-nucleon centre-of-mass system, f_{1i} and $\bar{f}_{2i}$ are the parton and antiparton distributions in nucleons, respectively, $\sum_i$ is a sum over all the parton types, such as $u\bar{u}$, $d\bar{d}$, $s\bar{s}$, $c\bar{c}$,..., λ_i is the charge of the i^{th} parton type, and x_1 and x_2 are the fractional momenta of parton and antiparton, respectively. A factor of 1/3 corresponds to the color degree of freedom. As $x_1=x_2=m/\sqrt{s}$ in the case of $y=0$, Eq. (I-3) is reduced to

$$\left.\frac{d^2\sigma}{dmdy}\right|_{y=0}=\frac{1}{m^3}f(m/\sqrt{s}) \qquad \text{(I-4)},$$

where s is the nucleon-nucleon c.m. energy squared. This cross section also exhibits scaling with respect to the scaling variable $\tau=m^2/s$.

The parton distribution function is known from the experiment of deep inelastic lepton-nucleon scattering; then, the antiparton distribution can be determined from the lepton pair mass spectrum in nucleon-nucleon scattering.

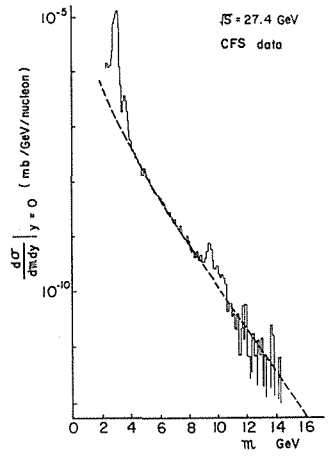

I-3

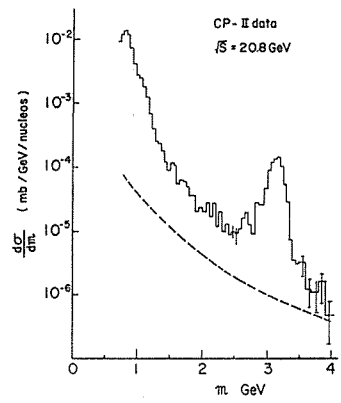

I-4

Fig. I-3 Mass distribution of CFS experiment compared with that of Drell-Yan prediction.
Fig. I-4 Mass distribution of CP-II experiment compared with that of Drell-Yan prediction.

So far, many experiments had been performed in the various regions of incident proton momentum and of lepton pair mass for both e^+e^- and $\mu^+\mu^-$ productions[1)6)~9)14)].

The Drell-Yan prediction of the dilepton continuum is in good agreement with the experiment in the high mass region ($m\gtrsim 4$ GeV), as is shown in Fig. I-3[7)]. On the contrary, in the low mass region ($m\lesssim 4$ GeV) the yield of muon pair is greater by a factor of 5 to 10 than that of Drell-Yan prediction, as is seen in Fig. I-4[8)].

Decays of vector mesons into lepton pairs and Dalitz decays from η^0 and ω^0 cannot account for the observed yield of low mass pairs. A few theoretical models were proposed to explain the copious production of low mass dilepton continuum[10)~13)]. For example, the idea proposed by Bjorken and Weisberg[10)] is that

the origin of this continuum is the annihilations of "wee" partons and antipartons produced in the collision process. This "soft" partons and antipartons produced in the collision process. This "soft" mechanism of lepton pair production is quite similar to those of mesons in hadron-hadron collisions[11][12].

The lepton pair data at low mass are scanty, especially for electron pair production[14]; therefore, it is necessary to study this process systematically to clarify the feature of this origin. This is the motivation of our experiment to study the reaction (I–1).

There are also interesting features in the reaction (I–2). The copious production of direct single leptons in hadron-hadron collisions at low p_T was observed with many experiments.[1] We are interested in the origin of direct single lepton production and the correlation between a copious production of single leptons and a large yield of lepton pairs.

This papers describes the experimental method and the data analysis for the reaction (I–1). The results of analysis are compared with the theoretical models.

II. Experimental Method

A. General

The experiment was performed at the slow-extracted beam line EP2–B of the National Laboratory for High Energy Physics (KEK). The overall view of the counter experimental hall of KEK at the time of this experiment is shown in Fig. II–1.

The 13-GeV/c protons extracted from the proton-synchrotron were directed to the EP2 beam line through a three-way beam splitting system. The external beam EP2–B was then focused onto a Be-target.

The principle element of experimental apparatus was a double-arm spectrometer

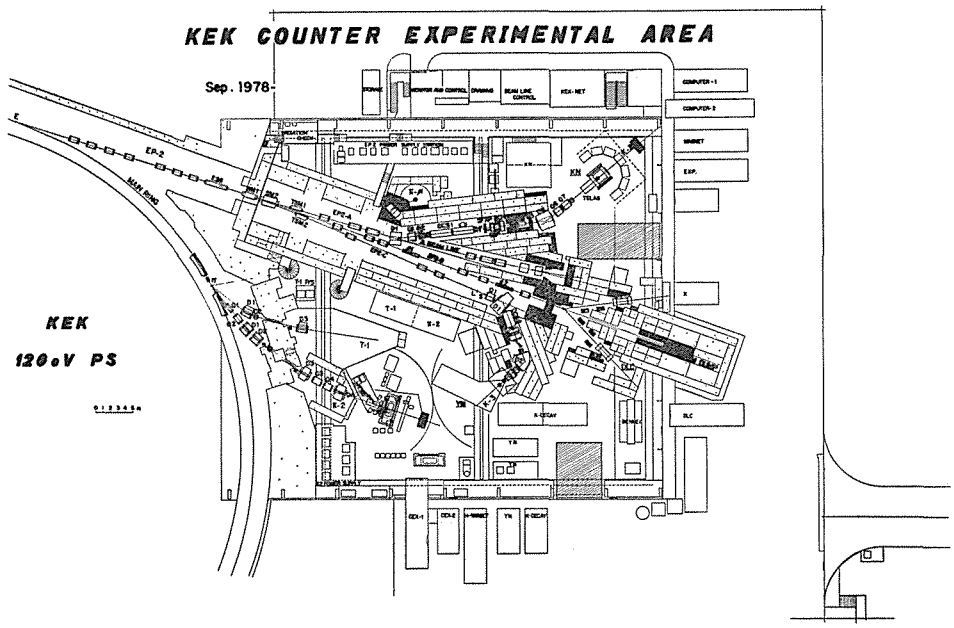

Fig. II–1 Overall view of counter experimental hall of KEK.

with two identical arms. Each arm consisted of an analysing magnet, multi-wire proportional chambers (MWPC), gas Čerenkov counters and a sampling shower counter.

Data were taken with a CAMAC system controlled by a NOVA-computer and then dumped onto magnetic tapes (MT). These MT data were analysed at the KEK central computer of HITAC-8800 by off-line.

In order to reduce the single counting rate of each arm and to achieve the coincidence pair-trigger rate as high as possible, we had no detector in front of the magnet and the target was enclosed in a helium box which extended to the front of the first detector.

The electron identification and hadron rejection was achieved by the use of two threshold-type gas Čerenkov counters and a sampling shower counter. This system was capable to reject hadrons by a factor of about 10^5.[15] The time difference between left and right arms was also measured to select the real electron-pair signals from background of two arm accidental coincidence.

The momenta of the produced particles were determined by the trajectries in the MWPC's and the field strength of the mganet, and then the value of the invariant mass of the electron-pair was calculated.

In order to deduce the cross section from the observed yield, the geometrical acceptance was calculated by a Monte-Carlo simulation.

B. Beam and Target

The 13-GeV/c circulating protons of the KEK proton-synchrotron were extracted by the resonant extraction system and then directed to the EP2 beam line through a three-way beam splitting system consisting of a static septum and a Lambertson magnet. The EP2 beam was splitted into three beam; EP2–A, EP2–B and EP2–C. The target was located downstream of EP2–B beam line. The beam height at the target position was 50 cm down from the level of circulating and extracted proton beams in order to reduce contamination associated with the beam halo.

A beam of intensity $1 \sim 3 \times 10^{10}$ protons per pulse and of spill time 300 msec was incident on the Be-target. The beam intensity was monitored by two secondary emission chambers (SEC), each located at 15 m upstream and 7 m downstream of the target. The numbers of incident protons on the target was monitored by a target-monitor; a scintillation counter telescope, placed at 90° with respect to the incident proton at 1.5 m from the target.

The horizontal and vertical sizes of the beam spot were monitored by a segmented wire ionization chamber (SWIC) placed at 0.5 m upstream of the target, where the beam size was 4 mm × 6 mm (FWHM) on the average.

The Be-target consisted of five pieces of segment; each segment was 12-mm wide, 40-mm high and 1.2-mm thick, and the total thickness was 6 mm. In order to reduce the external conversion of the γ-rays and the multiple Coulomb scattering, the target was enclosed in a helium box which was extended to the front of the first detector. The target, mounted on the movable stage, could be remotely positioned. In order to centre the incident proton beam on the target, the ratios of the target-monitor rate and of the coincidence rate of each arm to the SEC rate were measured as a function of the vertical and horizontal positions of the target.

C. Spectrometer

C–1. General

A double arm magnetic spectrometer has been built for the present experiment. The spectrometer consisted of two identical arms, each positioned at the same angle of 21° with respect to the beam, corresponding to θ cm$\simeq$90° in the proton-nucleon centre of mass system. Each arm of the spectrometer was composed of an analysing magnet, nine multi-wire propotional chambers (MWPC), two threshold-type gas Čerenkov counters (GC), a sampling shower counter (SSC) and three scintillation counters. The schematic view of the spectrometer is shown in Fig. II–2.

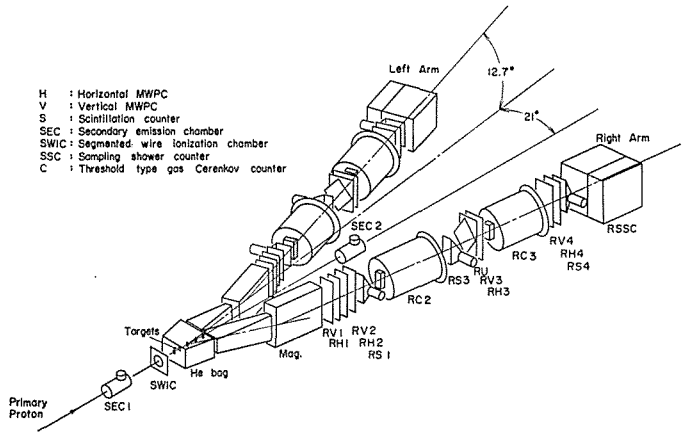

Fig. II–2 Schematic view of counter experimental setup.

The analysing magnet was a rectangular type dipole magnet with maximum field strength of 10 KG and the particle was bent vertically. The magnet was originally one of the standard beam line magnets at KEK and modified as the spectrometer magnet by removing a couple of coils to widen the aparture. The aparture was 100-mm wide, 400-mm high and 1.2-m long. The angular acceptance of each arm was $\pm$3.0° vertically and $\pm$0.5° horizontally.

As described before, no detector was placed upstream of the magnet and all the detectors were placed downstream of the magnet. Multi-wire proportional chambers were used to determine the outgoing trajectory of the secondary particles. The master trigger signals were generated by the coincidence of all the scintillation counters and the gas Čerenkov counters.

The timing signals, the pulse heights of each of the scintillation counters, of the gas Čerenkov counters, and the pulse heights of the shower counters together with the MWPC signals were recorded by a computer via CAMAC system and wirtten on magnetic tapes.

The momentum resolution $\Delta p/p$ was typically 2% and the mass resolution $\Delta m/m$ was 4% on the average. In the following subsection, the elements of the spectrometer will be described in detail.

C–2. Magnet

A window-frame type dipole magnet was used as an analysing magnet for the present experiment. The magnet was a standard element of KEK designed for the primary beam line, called 4D224 type. In order to convert the magnet to the spectrometer magnet, we removed a couple of coils from the magnet to widen the acceptance. The resulting aparture of the magnet was 100-mm wide, 400-mm high and 1.2-m long. As a result of removing the coils, the maximum field strength was reduced to about half of the original 4D224 magnet; to 10 KG at maximum. However, it was still sufficient since the magnet was operated at 4 KG and 9 KG during the experimentalr uns.

The result of magnetic field measurement is shown in Fig. II–3. The magnetic field was measured by using a Hall element by a stand-alone CAMAC system. The measured values of the magnetic field were finally dumped to MT for the later analysis.

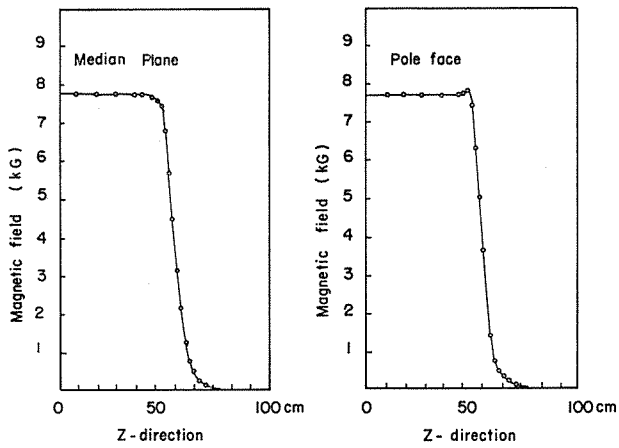

Fig. II–3 Field distribution of 4D224 magnet.

C–3. Multi-wire Propotional Chambers

In order to determine the trajectories of the secondary particles, it is necessary to measure the positions where the particles were passed through. We have used multi-wire proportional chambers (MWPC) to measure those positions; nine chambess were placed behind the magnet, four H-chambers (H1～H4), four V-chambers (V1～V4) and one U-chamber at each arm of the spectrometer. The H-chamber had the vertical sense wire plane to read out the horizontal coordinate, the V-chamber had the horizontal sense wire plane to read out the vertical coordinate, and the U-chamber had the wire plane rotated 20° with respect to the horizontal coordinate in order to reject the spurious multi-tracks.

We built four types of chambers of different sizes for this experiment; A, B, C and D-type chambers, and the B-type was used for the V-chamber, the C-type for the U-chamber and the D-type for the H-chamber. The frame size, the effective area and the other parameters of these chambers are shown in Table II–1.

The frame of MWPC was made of an epoxy glass plate. The Au-coated tungsten

Table II–1. Sizes of MWPC's and counters.

MWPC

TYPE	USAGE	EFFECTIVE AREA WIDTH×LENGTH	SPACE RESOLUTION	NUMBER OF CHANNELS
A		256×160	4	64
B	V	512×160	4	128
C	U	384×400	4	96
D	H	128×540	4	32

UNIT: mm

COUNTERS

NAME	SIZE		
	Width (mm)	Height (mm)	Thickness (mm)
S1	94	380	2
S3	112	500	2
S4	120	400	3

wires of 20-μm in diameter were used as the anode wires, and the copper-beryllium wires of 50-μm in diameter were used as cathode wires. The spacing of the sense wires was 2-mm and the read out spacing of them was 4-mm, respectively. The space resolution of MWPC was ± 4 mm on the average.

We used the LeCroy PCOS–II system as the read out system of MWPC. The system considted of 2700 controllers and 7700 chamber cards. Each chamber card contained amplifiers, discriminaters, delays and shift-registers for 32 channels. The card was mounted on the chamber directly. The signals were read out from the one side or from the both sides of the chambers. The chamber cards were connected serially with a flat-cable to the controller, and the wire-informations in the shift-registers were transferred to the controller serially. The block-diagram of PCOS–II system is shown in Fig. II–4.

The gas used in MWPC's was mixture of argon, isobutane and freon with methyral

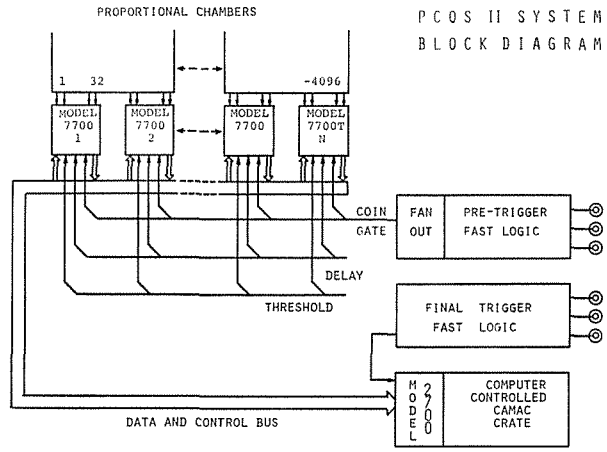

Fig. II–4 PCOS–II system block diagram.

vapor. The detection efficiencies of these chambers were approximately 95% with with the high voltage of 4.1 KV.

C–4. Gas Čerenkov counter[15]

The threshold-type gas Čerenkov counters were desgned and built to identify electrons or positrons in the hadronic background. The plan view of these counters is shown in Fig. II–5. We used two gas Čerenkov counters (C2 and C3) in each arm. These counters were placed at the spectrometer as shown in Fig. II–2.

Electrons which pass through the radiator in the counter and emit Čerenkov light. The emitted Čerenkov light was reflected by an aluminium coated spherical mirror by about 13° and collected to an RCA 8854 photomultiplier and gave an electrical signal.

Freon-12 gas was used as the radiator at the pressure of 1.1 atm and the temperature $\simeq$20°C which gave the threshold value 2.8 GeV/c for pion. The detection efficiencies of these counters were 97% on the average.

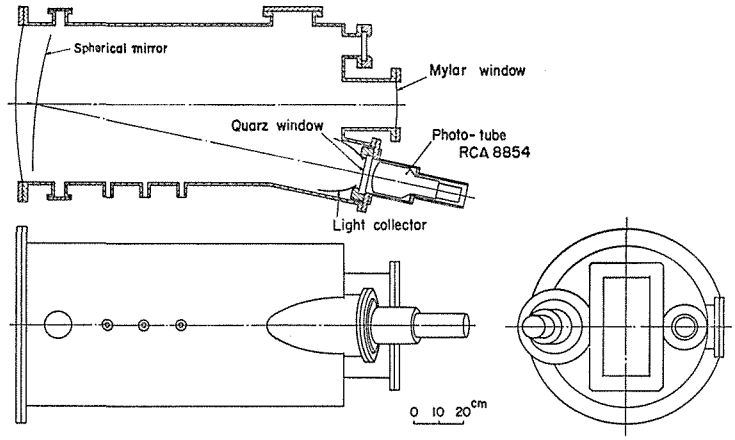

Fig. II–5 A construction of gas Čerenkov counter.

C–5. Sampling Shower Counter[15]

The sampling shower counters (SSC) were used for further electron identification and hadron rejection. The SSC was placed at the end of each arm of the spectrometer as shown in Fig. II–2.

Each shower counter consisted of three modules and was of 8.5 radiation length in total. One module had the seven layers of lead converters and the seven layers of scintillators, having a cross section of 20×50 mm^2 and 2.83 radiation lengths. Each module was viewed by two HTV R329 photomultipliers. The schematic view of one module of SSC is shown in Fig. II–6.

The pulse heights of SSC were analysed with the analogue to digital converters (ADC) and were stored in MT through the CAMAC system. The data of shower counters were only used for the off-line analysis.

The energy resolution was generally expressed as $\Delta E/E=32.5/\sqrt{E(\mathrm{GeV})}\%$ on the average. The hadron rejection factor of about 10^5 was achieved by using the present system consisted of two gas Čerenkov counters and the SSC.

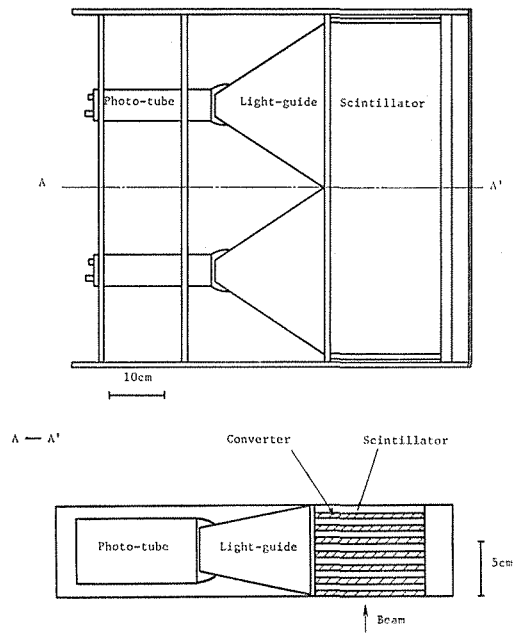

Fig. II–6 A construction of sampling shower counter.

C–6. Trigger Counter and Trigger Logic

Three scintillation counters (S1, S3 and S4) were used as the trigger counters. These counters were placed at the spectrometer as shown in Fig. II–2. As stated before, all these counters were placed behind the magnet in order to reduce the accidental rate and to ensure the high efficiency for the pair-trigger rate. The sizes of these scintillators are listed in Table II–1.

The trigger signal was generated according to the trigger logic as shown in Fig. II–7. The signal called "π"-signal was generated by the coincidence of scintillation counters; S1, S3 and S4, as defined in the following;

$$\text{"}\pi\text{"-signal} = S1 \cdot S3 \cdot S4.$$

The coincidence between "π"-signal and the signals of two gas Čerenkov counters, C2, and C3, was required to generate the "e"-signal, as defined in the following;

$$\text{"e"-signal} = S1 \cdot S3 \cdot S4 \cdot C2 \cdot C3.$$

The shower counter signal was not included in the master coincidence but latched in the register to give the pulse height information.

The two arm coincidence signal called "e^+e^-"-signal was generated by the coincidence between left and right arms as defined in the following;

$$\text{"}e^+e^-\text{"-signal} = (\text{"e"-signal in left}) \cdot (\text{"e"-signal in right}).$$

The "e^+e^-"-signal was used as the master signal to store all the informations into the computer and inhibited the fast logic for a period of 3 msec at most until these were stored.

Although the reate of the "e"-signals was fairly high, the rate of the "e^+e^-"-

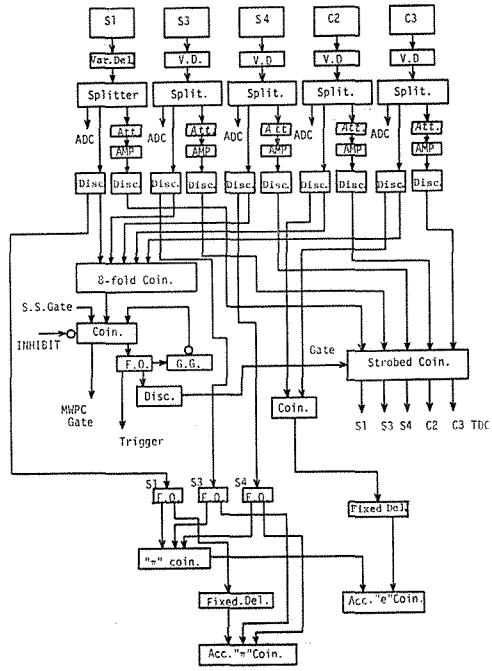

Fig. II–7 Block diagram of fast electronics.

signal was only about 0.1 events per burst. Therefore, in order to collect the data on single electron production simultaneously without loosing the collection efficiency of the electron-pair events, about five of the "e"-signals per arm were sampled during one pulse and added to the master signal.

The counts of inhibited "e^+e^-" events and of inhibited "e" events indicate the number of stored data of electron-pair event and that of single-electron event at one arm, respectively. The counts of non-inhibited "e^+e^-" events and of non-inhibited "e" events indicate the number of events of pair and of single electron at one arm and registered in the scalers, respectively. These data were used to correct the stored data due to the dead time losses. The accidental coincidence for "e^+e^-", "e", "π"-signals were also stored in the scalers to monitor the running condition.

D. Data Acquistion

The flow chart of data taking is shown in Fig. II–8. When the trigger signal was generated, the master coincidence was inhibited for a period of 3 msec at most until all the informations were stored in the computer, as described before. The master signal gated the chamber cards of PCOS–II system, and the position informations were stored in the shift-register, then the informations were read out with the contoroller serially. The master signal also gated the analogue to digital converters (ADC) and was used as the start pulse of the time to digital converters (TDC).

The informations, for example, the pulse heights and the timing signals of the scintillation counters and the gas Čerenkov counters, the pulse heights of SSC, the bit stauts of classifying the event, and the information of MWPC were stored in the computer, NOVA model 01, through the CAMAC system.

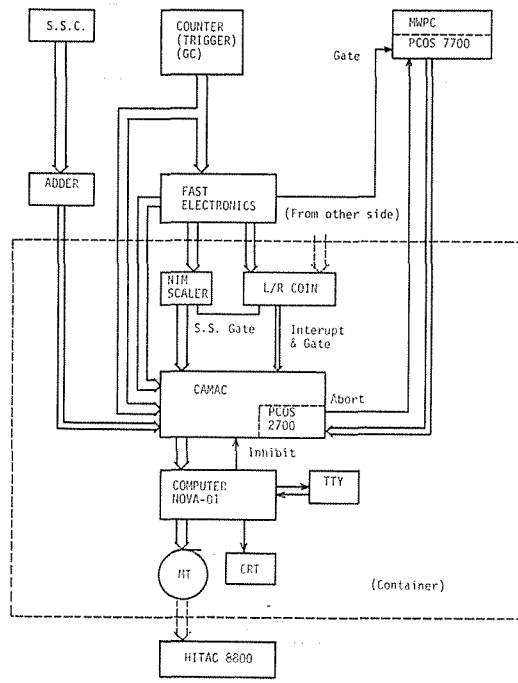

Fig. II–8 Flow chart of data acquistion.

The bit information of the coincidence register was used to classify the event type; whether the data were from the left or right arm, and of single-particle event or pair event. The data format of "event data" are shown in Table II–2. At the end of the beam spill, those data were dumped onto MT together with the "burst data", which contained the single counts of each counters, the beam intensity, the counts of target-monitor and other scaler data.

Various types of on-line display programs were employed to monitor the operation of the apparatus and are also shown in Table II–2. The on-line monitoring of the data taking was done by sampling the data in the event buffer. The histgram of interst could be displayed on the storage scope by calling the specified task from the disc.

The number of words per event depended on the multiplicity of MWPC data and its maximum number was truncated at 80 words. We discarded the data of over 80 words, as these were not possible to analyse and reconstruct trajectories.

The usable beam intensity was limited by the counting rate of the upstream trigger counter S1. The measurements were carried out by varying the beam intensity of the primary beam. The intensity of $1 \sim 3 \times 10^{10}$ protons per pulse gave the counting rate of the S1-counter about 1 MHz. A typical event rate of two arm coincidence was 0.3 sec^{-1} with the intensity of 2×10^{10} protons per pulse and the trigger rate of single-arm event was about 5 events at each arm per pulse because of the sampling trigger.

During the data taking, the beam condition was monitored by several informations such as the beam profile by SWIC, the shape of the beam spill and the ratios of the counting rate between two SEC's and between downstream SEC and the target monitor.

To avoid systematic errors, half of the data was taken at each polarity setting of

Table II–2. Read-in data format and CRT monitor.

DATA FORAT/EVENT/ARM

Run No.	1 word
Event No.	1
Run Parameters	8 words
ADC	8
SSC	12
TDC	8
Coin. Reg.	1
MWPC	$\leqq$40
SPARE	1
TOTAL	$\leqq$80 words (1 word=16 bits)

CRT — Monitoring

1) MWPC position distribution
2) ADC, SSC and TDC distribution
3) MWPC efficiency display
4) Scaler counts display
5) Event picture

the magnet. The magnetic field were chosen to be 4 KG and 9 KG, and these covered the ranges of electron-pair mass from 0.3 to 0.9 GeV, and from 06. to 1.3 GeV, respectively. Total incident protons on the target amounted to 2.6×10^{15} and 2.7×10^{15} at 4 KG and 9 KG magnet settings, respectively.

III. Data Reduction

A. General

The data stored in magnetic tapes (MT) were analysed by using the KEK central computer HITAC 8800.

As described before, the data taking was carried out in both the single particle trigger conditions and the pair trigger conditions, simultaneously. Therefore, the data in MT included both the single-arm-event data and the pair-event data. Because the most of the data in MT were those of single-arm events, only the pair-event data were selected and written on the pair data tapes (PDT) run by run. Scaler data were transferred onto PDT at the end of each run. As a result, about 200 MT's were reduced to 4 PDT's.

The particle trajectories of each event were reconstructed from the position information of MWPC and the momentum of the particle was calculated from this trajectories together with the field strength of the magnet.

Many criteria were imposed on the procedure of selecting genuine pair events from the reconstructed events. The cuts were applied on the distribution of the time difference (TOF) between left and right arms, the energy to momentum ratio (E/p) for the shower counter data, the horizontal vertex point at the target, and the vertical position of the trajectory in the magnet.

About 3.0 and 1.0×10^3 events of raw data for 4 KG and 9 KG settings were reduced to 70 and 20 events through the data reduction, resspectively.

The invariant mass of electron-positron pair was calculated for the event selected

by criteria listed above. The accidental backgrounds of two arm coincidence were estimated from the TOF spectrum between two arms, and were subtracted.

The geometrical mass acceptance of the spectrometer was calculated by a Monte-Carlo simulation which traced charged particles through the spectrometer. The multiple Coulomb scattering of the particles was included in this simulation.

The cross section $d^2\sigma/dmdy$ (per nucleon) at $y=0$ versus electron pair mass was derived from the corrected yield data by combining them with the geometrical mass acceptance.

Some of the above processes are described below in detail.

B. Data Processing

Since no detecter was used at the upstream of the magnet as described before, the particle trajectory was reconstructed using the position informations of MWPC placed at the downstream of the magnet.

The horizontal and vertical components of the trajectory were reconstructed separately by a straight line fit from each of four layers of MWPC (H1$\sim$H4, and V1$\sim$V4, respectively). If any of the horizontal or vertical component could not be reconstructed, such an event was discarded.

If several trajetories could be reconstructed from the data of MWPC's Hi and Vi, the deviation from the position of U-chamber, whose axis was rotated 20° with respect to the horizontal axis, was examined and the best one was adopted. For the events in which the deviation of the U-chamber position was too large or no tracks in the U-chamber, the best fitted tracks on both the horizontal and the vertical planes were chosen to be as the best fitted particle trajectory.

The left and right arm data of the two arm coincidence event were reconstructed by using the same track-reconstruction program. If the track in any one of each arm could not be reconstructed, such an event was of course discarded. The reconstruction efficiency of pair-event amounted to 62.5% in total.

The momentum of the particle detected at each arm was calculated from the best track selected by criteria described above.

We used only the vertical component of trajectory, because the error caused by neglecting the horizontal component is negligible for the momentum determination of the present experiment as the horizontal displacement is negligibly small comparing with the path length of track. We assumed that the particle was produced at the centre of the target because there was no detector before the magnet, and also assumed a hard edge magnetic field. The assumption of a hard edge magnetic field was justified by the measured magnetic field as shown in Fig. II–3.

The calculation of the momentum was done as described in the following; 1) the whole particle trajectory starting from the centre of the target to the straight line behind the magnet through the dipole magnet was reconstructed, 2) the value of momentum was computed by using the entrance and exit angles of the trajectory and the field strength of the magnet, according to the following equations;

$$\sin\alpha+\sin\beta=\frac{L}{\rho},$$

$$p=0.03\cdot B\cdot\rho,$$

where p=momentum of particle,
L=length of field section,

α = entrance angle,
β = exit angle,
B = field strength.

The procedures of selecting the genuine pairs from the reconstructed events were performed as follows, appling the cuts on the various quantities as mentioned before.

1) the time difference between left and right arms

Typical time difference distribution between two arms is shown in Fig. III–1. It shows the clear peak of the real electron-positron pairs over the accidental background distribution. The events under the peak were selected.

2) the energy to momentum ratio for the shower counter data

The energy to momentum ratio (E/p) was calculated by combining the energy of the particle obtained from the pulse height information of a shower counter and the momentum obtained from the magnetic spectrometer for each arm. Typical distributions of E/p, two-dimensional plot and one-dimensional histograms for both arms, are shown in Fig. III–2 and Fig. III–3, respectively. The event around unity of the value of E/p is that of electron-event. We selected the event which gave large E/p in the both arms.

3) the horizontal vertex point at the target

The target point distribution obtained from the extrapolation of the horizontal component of the trajectory was examined. Typical distributions of the target point at both arms are shown in Fig. III–4. The extrapolated track to target position was required to be in the target region. The events produced from the outside of this area were discarded and such backgrounds were mainly due to the electrons converted, scattered or produced from the magnet wall.

4) the vertical position of the trajectories in the magnet

The point of intersection of upstream and downstream tracks was also examined. The vertical components of the trajectories both in front of and behind the magnet were extrapolated into the region of the magnetic field. The point of intersection between these two extrapolated tracks must be in the vertical acceptance of the magnet.

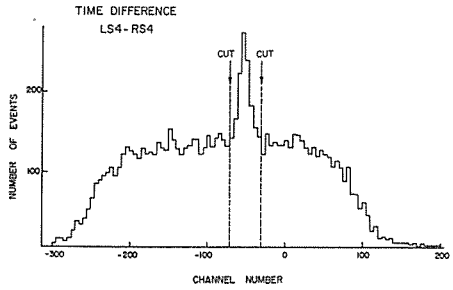

III–1

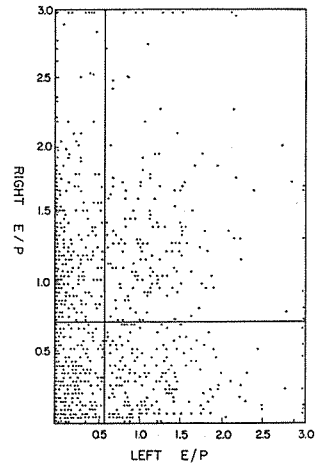

III–2

Fig. III–1 Typical distribution of time difference between left and right arms.
Fig. III–2 Typical destribution of scattered plot of E/p.

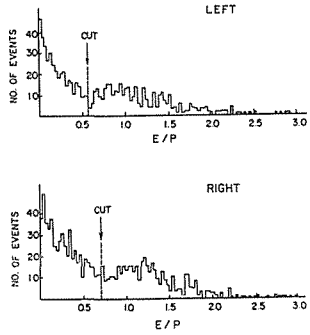

Fig. III–3 Typical distributions of E/p.

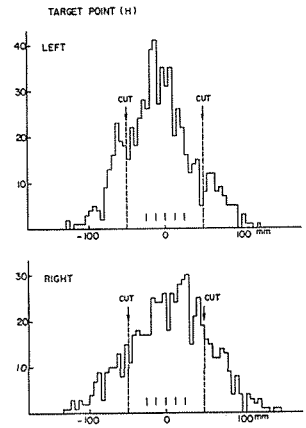

Fig. III–4 Typical distributions of target point.

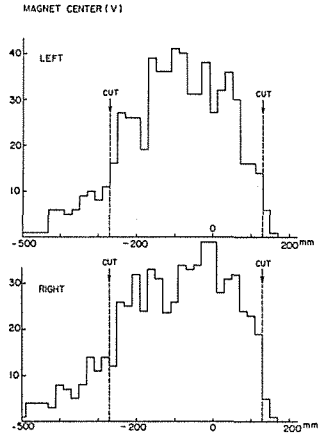

Fig. III–5 Typical distributions of point of intersection between upstream and downstream tracks.

Typical distributions of these quantities at both arms are shown in Fig. III–5. The events of which intersection point laid outside of this area were also dicarded with the same reason described above.

The invariant mass was computed for this selected event in the following,

$$m^2 = 2P_L \cdot P_R(1-\cos\theta_{LR}),$$

where m = invariant mass of electron-positron pair,
P_L = momentum of electron or positron in the left arm,
P_R = momentum of electron or positron in the right arm,
θ_{LR} = opening angle between the produced electron and positron.

The events caused from the accidental coincidence between two arms were still included in the selected events as is seen in Fig. III–1. Therefore, the invariant mass distributions of the backgound events were evaluated. The events outside of the peak in the time difference spectrum were arised from the accidental events. The

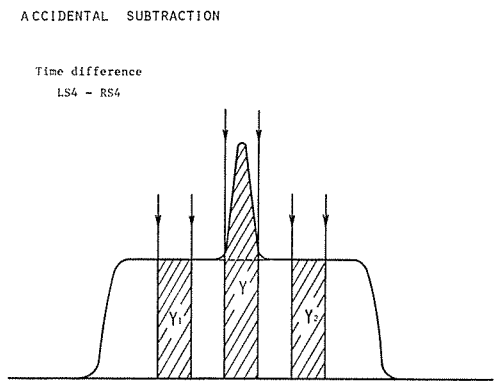

Fig. III–6 Accidental background subtraction.

events on the both side of the peak region, Y_1 and Y_2, as is shown in Fig. III–6 were also analysed and their invariant mass was computed by the same process described above. The yield caused from the accidental two arm coincidence (Y_B) was estimated with the following realtion,

$$Y_B = \frac{Y_1 + Y_2}{2} .$$

These accidental yield was subtacted, and finally the yield of the genuine electron-positron pair events were reduced. Furthermore, the yied were corrected for the dead time losses, the counter efficiency, reconstruction efficiency and cut efficiencies. The dead time losses were estimated to be 5% on the average by using the scaler data described in Sec. IIC–6. The loss of the counter efficiency was mainly due to the inefficiencies of the gas Čerenkov counters, which were 3% on the average as decribed in Sec IIC–4. The reconstruction efficiency was 62.5% in total as decribed in this section. The correction factor due to the TOF cut were estimated by fitting the TOF distribution by the Gaussian plus polynomial curves, and amounted to 93.8% in total. The E/p distribution was also fitted by the Gaussian plus exponential cuves for each arm. The correction factors due to this origin for the left and right arms were estimated to be 90.8% and 93.2% in total, respectively.

The cross section was obtained from these corrected yield. The mass distributions of electron-pairs for 4 KG and 9 KG magnet settings were shown in Fig. III–7.

C. Monte-Carlo Simulation

The geometrical mass acceptance was computed by a Monte-Carlo simulation by

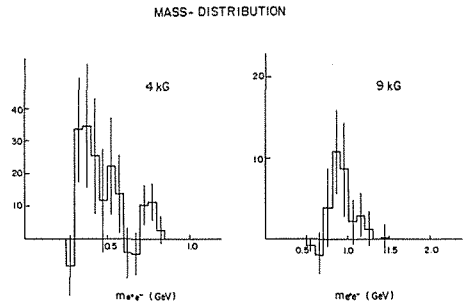

Fig. III–7 Mass distributions of raw events for 4 KG and 9 KG magnet settings.

tracing the trajectiries of the charged particles through the spectrometer.

An electron pair was generated by using the following assumptions, 1) a particle with mass (m), which was called "dilepton", was generaged in the target with the following transverse momentum (p_T) dependence[8];

$$E\frac{d^3\sigma}{dp^3}\simeq\exp(-b\cdot p_T),$$

and with the uniform distribution for the rapidity (y), and for the production angle (ϕ) in proton-nucleon centre of mass system, 2) This dilepton was decayed into electron pair isotropically in the rest frame of dilepton.

These generated electron and positron were traced through the spectrometer, where the multiple scattering due to all the materials in the spectrometer were taken into account and the hard edge magnetic field was assumed again. This simulation was done for both 4 KG and 9 KG magnet settings.

The geometrical mass acceptance and the y-acceptance of the present spectrometer are shown in Fig. III–8 and Fig. III–9, respectively. Since the present data were distributed at $y=0\pm0.05$, the present measurements were performed arround the region of $y=0$.

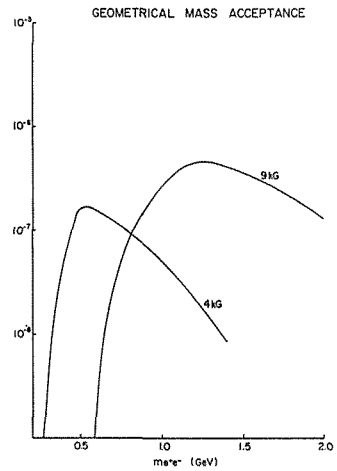

Fig. III–8 Geometrical mass acceptance of the spectrometer.

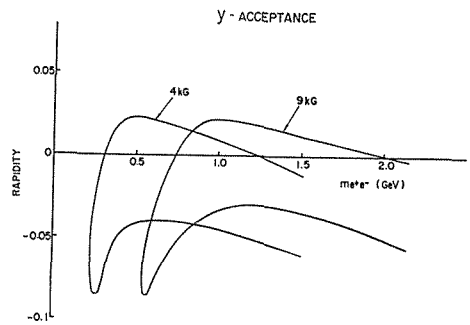

Fig. III–9 y-acceptance of the spectrometer.

D. Calculation Cross Section

The differential cross section $d^2\sigma/dmdy$ (per nucleon) at $y\simeq 0$ was deduced from the corrected yield and the geometrical mass acceptance by using the following formula,

$$\frac{d^2\sigma}{dmdy}=\frac{1}{IN_A\rho l}\cdot\frac{A}{A^{2/3}}\cdot\frac{1}{A(m,\,y)}\cdot\frac{\Delta Y}{\Delta m\Delta y},$$

where
A = atomic weight of Be = 9.01,
ρ = density of Be = 1.848 gram/cm,
l = target length = 6 mm,
N_A = Avogadro's number,
I = total mumber of protons incident on the target,
$A(m,\,y)$ = geometrical acceptance,
Y = corrected yield.

Losses due to nuclear absorption within the target amounted to 0.8% and were neglected. To obtain the cross section per nucleon, the $A^{2/3}$-dependence was assumed. This is justified for low mass pair production[8].

IV. Results and Discussions

A. Experimental Results

In Table IV–1 we present the observed cross sections per nucleon versus electron pair mass obtained by the present experiment for the reaction,

$$p+Be \longrightarrow e^+e^-+X \qquad \text{(IV–1)},$$

at the incident proton momentum of 13 GeV/c. The cross sections are also shown in Fig. IV–1. The errors presented here include only the statistical errors. The statistical errors of the Monte-Carlo simulation were less than 4% at maximum and were negligibly small compared with those of the observed data. The systematic error was mainly due to that of the incident proton number measured by the secondary emission chamber (SEC). SEC was calibrated by the current transformer (CT) at the fast-extracted beam line of the KEK proton synchrotron. The error of SEC was $\pm 20\%$ at maximum. Therefore, the differential cross section of the present experiment contains $\pm 20\%$ systematic error for the absolute normalization.

Dalitz pairs from $\eta^\circ\rightarrow\gamma e^+e^-$ and $\omega^\circ\rightarrow\pi^\circ e^+e^-$ might contribute to low mass electron pairs at masses below ρ° and ω°. We examined these contiibutions by a Monte-Carlo simulation for the present experimental configuration. The results indicate that the above contributions were less than 1% of the observed yield at maximum and these were negligibly small, unlike the case for an experiment with wider acceptance.

The present results cover the electron pair mass region of $0.3\leq m_{e^+e^-}\leq 1.3$ GeV and the rapidity arround $y=0$.

The mass spectrum $d^2\sigma/dmdy$ (per nucleon) at $y=0$ consists of the continuum part and the peak around 775 MeV which is due to $\rho^\circ(\omega^\circ)\rightarrow e^+e^-$.

The differential cross section of the inclusive ρ° production was computed from the present data. The result was given by

$$B\frac{d\sigma}{dy}\Big|_{y=0}\simeq(4.02\pm 0.12)\times 10^{-5}\,\text{mb/nucleon},$$

Table IV–1. Cross section of the reaction (IV–1).

Cross section of the reaction; $p+Be \rightarrow e^+e^-+X$

$\left.\frac{d^2\sigma}{dmdy}\right|_{y=0}$ $\quad -0.05 \leq y \leq 0.05$

$\sqrt{s} = 5.12$ CeV

(The unit of the cross sections = mb/GeV/nucleon)

4 KG

$m_{e^+e^-}$ (GeV)	$\left.\frac{d^2\sigma}{dmdy}\right\|_{y=0}$
0.325±0.025	$80.71 \pm 39.65 \times 10^{-4}$
0.375	24.85±13.81
0.425	8.47± 5.97
0.475	1.80± 2.46
0.525	2.58± 1.73
0.575	2.12± 1.84
0.725	2.37± 1.40
0.775	2.81± 1.76
0.825	0.74± 1.04

9 KG

$m_{e^+e^-}$ (GeV)	$\left.\frac{d^2\sigma}{dmdy}\right\|_{y=0}$
0.85±0.05	$95.86 \pm 46.15 \times 10^{-6}$
0.95	47.00±30.86
1.05	7.02± 9.15
1.15	8.17± 7.45
1.25	3.08± 4.98

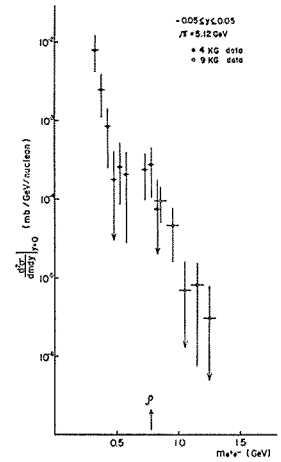

Fig. IV–1 Cross section for the reaction (IV–1) versus electron pair mass. ● and ○ represent the data obtained with the 4 KG and 9 KG settings, respectively.

where B is the branching ratio into e^+e^-. The inclusive ρ° production was studied in a bubble chamber experiment with proton-proton collision at 12 GeV/c[16]. They obtained,

$$\left.\frac{d\sigma}{dy}\right|_{y=0} \simeq 1 \text{ mb.}$$

Using the value of the Particle Data Group[17] for $B(\rho^\circ \to e^+e^-)$, which is $(4.3 \pm 0.5) \times 10^{-5}$, this gives

$$\left. B\frac{d\sigma}{dy}\right|_{y=0} \simeq 4.3 \times 10^{-5} \text{ mb.}$$

This value is consistent with the present result.

B. Discussions on Continuum

B–1. Drell-Yan Model

As described in Chapter I, the Drell-Yan type quak-parton annihilation models[5] well predict the high mass ($m \gtrsim 4$ Gev) dilepton continuum. However in the low mass region ($m \lesssim 4$ Gev), the predicted cross sections differ from the observed cross sections by a factor of 5 to 10 for muon pairs.

The Drell-Yan cross section given by Eq. (I–4) can be expressed explcitly by the following equation[12],

$$\left. m^3 \frac{d^2\sigma}{dm dy}\right|_{y=0} = C_{DY}\left(1 - \frac{m}{\sqrt{s}}\right)^{10} \qquad \text{(IV–2)},$$

with $C_{DY} = 1.3 \times 10^{-5}$mb $\cdot$ Gev^2. The power 10 in Eq. (IV–2) is arised from dimensional arguments of parton distributions, and the normalization factor C_{DY} is determined from the experimental results on deep inelastic lepton-nucleon scattering.

In Fig. IV–2, the Drell-Yan prediction calculated from Eq. (IV–2) is illustrated with the present results. The present results indicate that the yield of low mass electron pairs is about one order of magnitude greater than that of the Drell-Yan process as same as the low mass muon pairs. This fact suggests that the low mass continuum is originated from diffent mechanism.

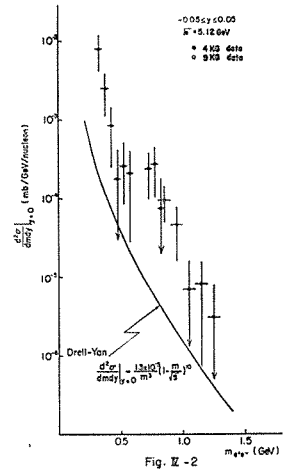

Fig. IV–2 Simple extrapolation of Drell-Yan prediction compared with our data.

B–2. Models for Low Mass Continuum

In order to over come the difficulties at low mass region, Bjorken and Weisberg[10] modified the Drell-Yan mechanism for the low mass region by introducing the many "wee" partons and antipartons "produced" in the collision process. These partons and antipartons reannihilate into leptons before the products of collision emerge. They showed qualitatively that this modification gave the larger cross sections than the original Drell-Yan mechanism.

Černý et al.[11] proposed that dileptons produced in hadron-hadron collisions consist of two components. In addition to the Drell-Yan process, they added the process of annihilations of quark-antiquark pairs created during the collision, which is responsible to production of low mass dileptons. These quarks ($q's$) and antiquarks ($\bar{q}'s$) are created druing the space-time evolusion of the collision, and $q's$ and $\bar{q}'s$ in different rapidity regions are created in different time. This constraint suppresses annihilations of q and $\bar{q}$ separated by a large rapidity gap and leads to the production of low mass dileptons.

In the calculations of the yield of the Drell-Yan component and the added low mass component, the finite mass and transverse momenta of $q's$ and $\bar{q}'s$ are taken into account. The distibutions of quarks created during the collision are obtained basing on their Monte-Carlo quark-parton model of multiple production.

Their results of dimuon mass spectrum can reproduce well the Chicago-Princeton II[8] data of the low mass spectrum for the reaction at 150 GeV/c. Their low mass component is much larger than the Drell-Yan component.

Černý et al.[18] have calculated the yield of electron pairs under the presetn experimental condition by the Monte-Carlo simulation. The preliminary results are shown in Fig. IV–3 and Fig. IV–4 together with the present results. The histgram in Fig. IV–3 are obtained with the quark mass of 0.01, 0.01, and 0.15 GeV for u, d, and s quarks, respectively. In Fig. IV–4, the quark masses are fixed at 0.1, 0.1, and 0.25 GeV.

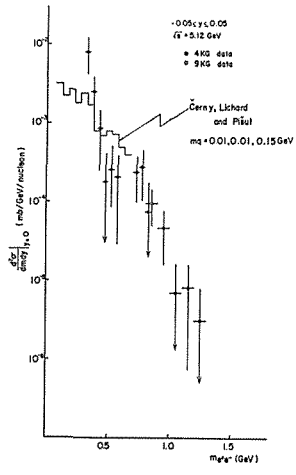

Fig. IV–3

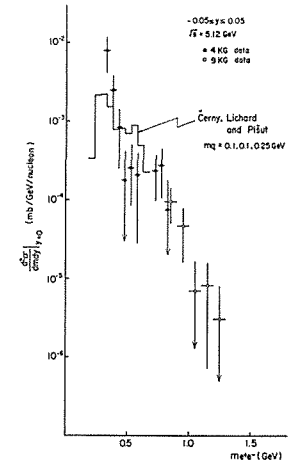

Fig. IV–4

Fig. IV–3 and 4 Preliminary calculations by Černý et al. with quark mass 0.01, 0.01 and 0.15 GeV and with 0.1, 0.1 and 0.25 GeV for u, d and s, respectively.

This model can explain the copious production of low mass electron pairs found in the present experiment. However, the calculation should be extend to high mass region above 1 GeV to confirm the validity of this model.

Kinoshita et al.[12] proposed the hadronlike model for dilepton production in hadron-hadron collisions. In this model, they assumed that the functional behavior of the transverse- and longitudinal-momentum spectra of virtual photons, their dependences on the incident energy, all the relevant parameters of these distributions, are the same as low-p_T hadron physics.

They formulate the yield of the dilepton mass continuum from their hadronlike model as the following equation,

$$\frac{1}{g(m)} \cdot \frac{\mathrm{d}^2\sigma}{\mathrm{d}m\mathrm{d}y}\bigg|_{y=0} = \left(1-\frac{m}{\sqrt{s}}\right)^7 \qquad \text{(IV–3)},$$

To specify the function $g(m)$ in Eq. (IV–3), they introduce a power ansatz, $g(m)\sim m^{-\beta}$, which contains the free parameter β. They determine the absolute normalization and mass dependence from the experimental results of the dimuon production by the Chicago-Princeton II collaboration. However, the CP–II experiment was not performed at $y=0$. Therefore, their carbon data taken at $x_F \gtrsim 0.1$ are extrapolated to $y=0$ in their analysis. The following parameter for $g(m)$ were determined by this analysis,

$$g(m)=\frac{C}{m^5}, \quad \text{with} \quad C=1\times10^{-3}\ \mathrm{mb}\cdot\mathrm{GeV}^4.$$

This formula gives about ten times larger cross sections, when we compare with the present results on production of the low mass electron pairs, as is shown in Fig. IV–5. Furthermore, the predicted mass spectrum has rather steep mass dependence than the experimental results.

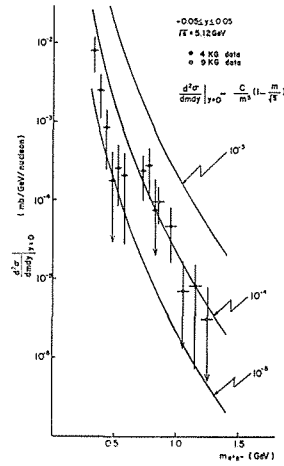

Fig. IV–5

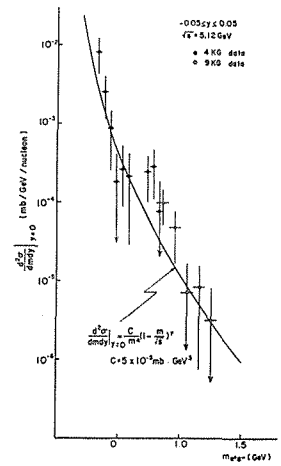

Fig. IV–6

Fig. IV–5 Theoretical predictions of Eq. (IV–3) where the normalization constant C is chosen to be 1×10^{-3}, 1×10^{-4}, 1×10^{-5}.

Fig. IV–6 Theoretical predictions of Eq. (IV–4) where the normalization constant is chosen to be 5×10^{-5}mb·GeV^3.

Kinoshita[19] has suggested that in the lower mass region m^{-4} behavior seems to be appropriate rather than original m^{-5} behavior of $g(m)$. Then we compare the present results with the following formula,

$$m^4 \frac{d^2\sigma}{dmdy}\Big|_{y=0} = C\left(1-\frac{m}{\sqrt{s}}\right)^7 \qquad \text{(IV–4)}.$$

Fig. IV–6 shows the comparison of the present results with the prediction. The best fit is obtained by choosing C to be 5×10^{-5} mb·GeV^3.

Adachi and Yotsuyanagi[13] have also developed two-component model for dilepton production in hadron-hadron collisions. They consider the model which unifies two different mechanisms: the Drell-Yan process and the process proposed by Bjorken and Weisberg. They try to unify these two different mechanisms by solving the equation of evolution of probability distribution with the time evolution of collision process.

Immediately after hadronic collisions occured, a hot matter called hadronic matter, is created at a thermal unstable state and alsmost no hadrons are yet created. In this stage, high-p_T hadrons and high mass virtual photons are created by "hard" interaction of constituents with momenta almost the same as those of incident hadrons. Free constituent picture is likely to be good for this process. Then at the time after interactions have been transmitted to the extent of hadron size, hadronic matter expands and is cooled and then is to be a thermal stable state by weekening the interaction with each other. Many hadrons are produced. Low-p_T hadrons and low mass virtual photons are created by "soft" interactions of constituents produced in the collision process. The dynamics described by hadronic or thermodynamic picture is seemed to be dominated in this stage.

As described before, these authers are trying to unify these two diffent mechanisms by using Boltzman's equation of time-evolution. The predictions based on their model reproduce the dilepton mass continuum of the Chicago-Princeton II[8] and the Colombia-Fermilab-Storny brook[7] experiment fairly well.

Adachi and Yotsuyanagi[20] have calculated the electron pair mass continuum for the present experimental condition. The preliminary result of their calculation is

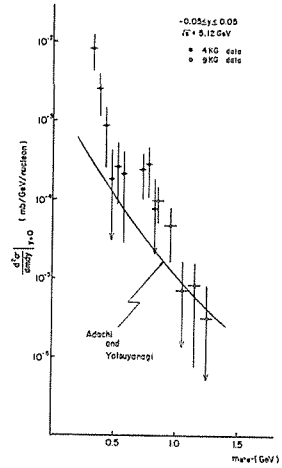

Fig. IV–7 Preliminary calculation by Adachi and Yotsuyanagi.

shown in Fig. IV–7 together with the present results. The calculated value shows rather flat dependence on the pair mass and smaller than the present results.

B–3. Comment on Bremsstrahlung Mechanism

The origin of dilepton is a virtual photon which converts in to a lepton pair. There is a possibility that virtual photons are created by bremsstrahlung from charged constituents during the collisions beside an annihilation mechanism.

However, the real photons associated with the bremsstrahlung mechanism. Furthermore, the bremsstrahlung mechanism implies a dilepton mass distribution to be $d\sigma/dm \sim 1/m$ for small m. A number of leptons must be proportional to $\log(m_{max}/m_i)$. The e/μ ratio would then be $\sim \log(m_{max}/m_e)/\log(m_{max}/m_\mu)$. For $m_{max} \lesssim 1$ GeV, we should have $e/\mu \gtrsim \log 10^3/\log 10 = 3$.

As described before, the present experimental results show the electron pair mass distribution are proportional to m^{-4}, and is incosistent with the bremsstrahlung mechanism.

V. Conclusions

The mass distribution of the electron pair production in proton-nucleus collisions was obtained in the mass region between 0.3 and 1.3 GeV at $y=0$ with the incident momentum of 13 GeV/c.

The present results indicate that the yield of low mass electron pair is more copious than the due to Dreil-Yan process, suggesting that the low mass continuum is originated from different mechnisms.

The m^{-4} behavior of hadron-like model formulated by Eq. (IV–4) reproduces the mass distribution of the present results. This suggests that the "soft annihilation" mechanism is a dominant source of copious yield of low mass lepton pairs produced in hadron-hadron collisions. The virtual photon bremsstrahlung mechanism seems to be difficult to explain the results.

There remains still quantitative uncertainties in both theoretical and experimental analyses. To distinguish the possible mechanisms for low mass continuum, more precise data on s-dependence, p_T-dependence, x_F-dependence, μ–e difference and others are required.

ACKNOWLEDGEMENTS

This experiment has been performed under the supervision of Prof. S. Mikamo. His guidance, suggestion and encouragement in this work are acknowledged. The author also would like appreciate Prof. A. Kusumegi for his support, guidance and encouragement during this work at KEK. Thanks are also due to Dr. A. Maki for his support, guidance, encouragement and partnership in the almost all the stage of this experiment. Without him, this experiment would never have been completed.

The author would like to express his thanks to Prof. K. Miyake and to the members of high energy physics laboratory of Kyoto University for their continuous encouragements and guidances through his graduated course.

He is grateful to Dr. M. Ono, Dr. J. Kishiro and Mr. Y. Sakai for their partnership in the preparation, in the data taking and in the data analysis of this experiment. Thanks are also due to Prof. M. Mishina, Prof. T. Ishizuka and the members of high

energy physics laboratory of Osaka City University under Prof. S. Ozaki, Prof. S. Higashi and Prof. T. Takahashi for their collaborations during this experiment.

His thanks are also due to the members of the beam channel group of KEK under Prof. H. Hirabayashi for their co-operations and efficient operation of the beam line and for their helpful suggestions and discussions.

The accomplishment of this experiment is also attributed to the proton synchrotron crew under Prof. Y. Kojima at the Accelerater Department of KEK. Their efficient operation of proton synchrotron is much appreciated. His thanks are also due to the members of the data handling division under Prof. H. Takahashi for developing the off-line analysis programs and to those of the workshop under Prof. T. Hongo for fabrication of the detectors and the mechanical instruments.

His thanks are also due to Prof. S. Suwa of the Physics Department of KEK for his encouragement and support in achieving this experiment.

REFERENCES

1) L. M. Lederman, Physics Reports **26C** (76), 151.
N. S. Craigie, Physics Reports **47C** (78), 1.
K. Kinoshita, Soryushiron Kenkyu (Kyoto) **56** (78), 91 (in Japanese)
2) For recent review see:
O. Nachtmann, Lepton photon Sympo., Hamburg, 1977, p. 811.
3) For recent review see:
G. J. Feldman, Proc. of 19th Intl. Conf. on High Energy Physics, Tokyo Japan, 1978, p. 777.
4) J. D. Bjorken, Phys. Rev. **179** (69), 1547.
J. D. Bjorken and E. A. Pachos, Phys. Rev. 185 (69), 1975.
5) S. D. Drell and T. M. Yan, Phys, Rev. Lett. **25** (70), 316;
Ann. Phys. (N. Y.) **66** (71), 578.
6) For recent reviews see:
L. M. Lederman, Proc. of 19th Intl. Conf. on High Energy Physics, Tokyo Japan, 1978, p. 706.
J. W. Cronin, Lepton Photon Sympo., Hamburg, 1977, p. 576.
7) Colombia-Fermilab-Storny Brook Collaboration:
D. C. Hom et al., Phys. Rev. Lett. **36** (76), 1236.
D. C. Hom et al., Phys. Rev. Lett. **37** (76), 1374.
S. W. Herb et al., Phys. Rev. Lett. **39** (77), 252.
W. R. Innes et al., Phys. Rev. Lett. **39** (77), 1240.
8) Chicago-Princeton II Collaboration:
K. J. Anderson et al., Phys. Rev. Lett. **37** (76), 799, 803.
J. G. Branson et al., Phys. Rev. Lett. **38** (77), 1331, 1334.
9) BNL-Yale Collaboration:
W. M. Morse et al., Phys. Rev. **D18** (78), 3145, 3150.
10) J. D. Bjorken and H. Weisberg, Phys. Rev. **D13** (76), 1405.
11) V. Černý, P. Lichard and J. Pisut, Phys. Lett. **70B** (77), 61.
12) K. Kinoshita, H. Satz and D. Schildknech, Phys. Rev. **D17** (78), 1834.
13) T. Adachi and I. Yotsuyanagi, to be published.
14) J. H. Cobb et al., Phys. Lett. **78B** (78), 519.
A. Chilingarov et al., Nucl. Phys. **B151** (79), 29.
15) Y. Sakai, Master Thesis (in Japanese), 1979.
16) V. Blobel et al., Phys. Lett. **48B** (74), 73.
17) Particle Data Group, "Review of Particle Properties", LBL-100, April, 1978.
18) V. Černý, private communication.
19) K. Kinoshita, private communication.
20) I. Yotsuyanagi, private communication.